Gondwana Research 129 (2024) 23–35

Contents lists available at ScienceDirect

Gondwana Research

journal homepage: www.elsevier.com/locate/gr

50° Post-Eocene clockwise rotation of Mangkang and its implications for the oroclinal bending of the southeastern Tibetan Plateau

Wanlong Xu [a,b,c], Maodu Yan [a,b,*], Douwe J.J. van Hinsbergen [c], Bingshuai Li [d], Chong Guan [e], Qiang Fu [a,c], Liang Yu [f], Zunbo Xu [a,b], Dawen Zhang [g], Miaomiao Shen [a], Zhantao Feng [a], Zhichao Niu [a,b], Bram Vaes [c]

[a] State Key Laboratory of Tibetan Plateau Earth System, Environment and Resources (TPESER), Institute of Tibetan Plateau Research, Chinese Academy of Sciences, Beijing 100101, China
[b] University of Chinese Academy of Sciences, Beijing 100049, China
[c] Department of Earth Sciences, Utrecht University, Utrecht 3584CS, the Netherlands
[d] School of Earth Sciences, East China University of Technology, Nanchang 330013, China
[e] Xi'an Center of Geological Survey (Northwest China Center of Geoscience Innovation), China Geological Survey, Xi'an 710054, China
[f] School of Ecology, Resources and Environment, Dezhou University, Dezhou 253023, China
[g] School of Tourism, Resources and Environment, Zaozhuang University, Zaozhuang 277160, China

ARTICLE INFO

Article history:
Received 31 January 2023
Revised 12 November 2023
Accepted 9 December 2023
Available online 14 December 2023
Handling Editor: J. Meert

Keywords:
Paleomagnetic rotation
Mangkang
Late Eocene
Oroclinal bending
Crustal shortening

ABSTRACT

The extrusion and clockwise rotation of the southeastern Tibetan Plateau around the Eastern Himalaya Syntaxis has been playing an important role in accommodating the Tibetan Plateau lithosphere shortening. Establishing the extrusion and rotation processes has great significance in understanding the still hotly debated deformation of the Tibetan Plateau. Here we conduct a new paleomagnetic study of the Upper Eocene (~33.4–36.4 Ma) volcanogenic rocks from Mangkang (29.7°N, 98.6°E), which is located in the eastern Qiangtang Terrane that bent around the Eastern Himalaya Syntaxis. A total of 184 characteristic remnant magnetizations of 20 sites were identified and have a tilt-corrected site-mean direction of Ds = 62.2 ± 5.5°, Is = 47.6 ± 5.7°, K = 46.7, A_{95} = 4.8°. The statistical properties of the obtained paleomagnetic directions can be straightforwardly explained by paleosecular variation, together with a positive fold test, yielding likely Late Eocene primary magnetizations. Integrated with other available paleomagnetic results and geological evidence in the adjacent areas, we speculate that there existed a ~ 50° clockwise rotation of the Mangkang area with respect to the Eurasian Plate after the Late Eocene, due to the oroclinal bending around the Eastern Himalaya Syntaxis. The paleolatitudes estimated from paleomagnetic results indicate that the area between Eurasian and eastern Qiangtang has experienced significant latitudinal crustal shortening during the Eocene, which is consistent with geological evidence.

1. Introduction

The Tibetan Plateau was formed by the subduction of the India Plate underneath the Tibetan Plateau lithosphere and subsequent collisions of India with Eurasia, which have generated massive crustal shortening and spectacular uplift during the Cenozoic (Fang et al., 2020; Tapponnier et al., 2001; van Hinsbergen et al., 2012; Yin and Harrison, 2000). It is the natural laboratory to study the geodynamics process governing plateau rise and tectonic-climate coupling (Molnar and England, 1990; Tapponnier et al., 2001; van Hinsbergen, 2022; Yin and Harrison, 2000). During the India-Eurasia collision, the southeastern Tibetan Plateau has experienced significant clockwise rotation and southeastward extrusion along the Eastern Himalaya Syntaxis (EHS), as a result of Tibetan lithospheric shortening relative to the stable South China Block (Chung et al., 1997; Leloup et al., 2001; Li et al., 2017a; Replumaz and Tapponnier, 2003; Searle, 2006; Tapponnier et al., 1982; Tong et al., 2013, 2021; Yang et al., 2001; van Hinsbergen et al., 2011b) (Fig. 1a). Therefore, understanding the deformation history of the southeastern Tibetan Plateau is vital in assessing the still hotly debated processes and mechanisms of the Cenozoic tectonic evolution of the entire Tibetan Plateau.

Many studies have been conducted on the Cenozoic tectonic deformation of the southeastern Tibetan Plateau, such as the extrusion and rotation of the Lanping-Simao-Indochina Terrane along the Ailao Shan-Red River Fault (ASRRF) (Fig. 1). It was widely accepted that the left-lateral movements of the ASRRF occurred

* Corresponding author.
E-mail address: maoduyan@itpcas.ac.cn (M. Yan).

https://doi.org/10.1016/j.gr.2023.12.004
1342-937X/

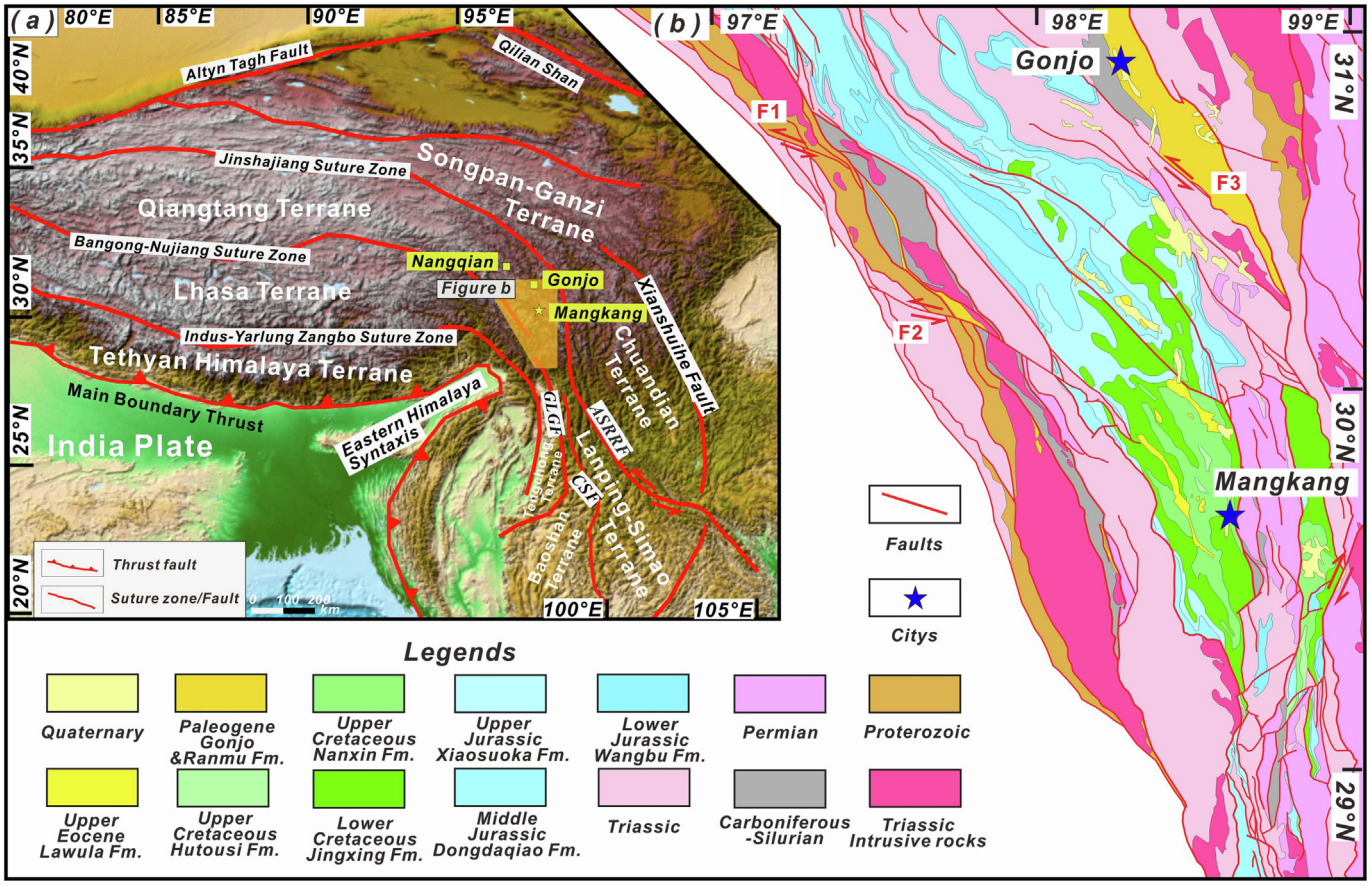

Fig. 1. (a) Simplified tectonic map of the Southeastern Tibetan Plateau and its adjacent regions. The orange shadow area is shown in b. (b) Schematic geological map of the Mangkang and surrounding areas. The abbreviations of the tectonic units are ASRRF: Ailao Shan-Red River Fault; CSF: Chongshan Fault; GLGF: Gaoligong Fault. (For interpretation of the references to colour in this figure legend, the reader is referred to the web version of this article.)

during 35–17 Ma (Harrison et al., 1996; He et al., 2020; Leloup et al., 1995; Tapponnier et al., 2001; Zhang et al., 2014), with significant clockwise rotation of the Lanping-Simao-Indochina Terrane since the Late Eocene (e.g., Li et al., 2017a; Sato et al., 1999; Tanaka et al., 2008; Tong et al., 2013; Yang et al., 2001). However, these reported activities occurred significantly later than the initial collision of India with Eurasia around the EHS at ~ 50 Ma (Baral et al., 2019). The estimated amount of extrusion varies largely, from more than 1000 km to only 250 km, either by the left-lateral strike-slip displacements along the ASRRF (Chung et al., 1997; Leloup et al., 2001; Mazur et al., 2012) or the paleolatitude differences between the South China Block and the Lanping-Simao Terrane (Gao et al., 2015; Li et al., 2017a; Sato et al., 1999; Tanaka et al., 2008; Yang et al., 2001). The southeastern Tibetan plateau was deformed either through large-scale or small-scale extrusions, which the former would place the Lanping-Simao-Indochina Terrane in between the Qiangtang and Lhasa terranes before extrusion (Replumaz and Tapponnier, 2003; Royden et al., 2008), while the latter implies the Lanping-Simao-Indochina Terrane was the eastern extension of the Qiangtang Terrane (Hall, 2002; van Hinsbergen et al., 2011a). Paleomagnetic declination analyses revealed various magnitudes of clockwise rotations ranging from 0° to 80° or even counterclockwise rotation of the Lanping-Simao Terrane since the Late Eocene, resulting in ideas of localized internal deformation of a single terrane (Gao et al., 2015; Tanaka et al., 2008; Tong et al., 2013) or independent rigid deformation of several micro-terranes (Li et al., 2017b).

Some paleomagnetic studies have been carried out in the Nangqian-Qamdo-Gonjo region north of the EHS (Fig. 1a) (Huang et al., 1992; Li et al., 2020; Otofuji et al., 1990; Tong et al., 2015, 2017; Zhang Y. et al., 2018; Zhang W. et al., 2020). Complicated Eocene rotations have been observed in this region, such as three episodes of different senses of rotation (e.g., clockwise, insignificant, or counterclockwise), due to the southeastward extrusion and clockwise rotation of the southeastern Tibetan Plateau (Li et al., 2020; Zhang Y. et al., 2018; Zhang W. et al., 2020), or due to oroclinal bending around the EHS (Todrani et al., 2021). It indicates that the deformation in the Nangqian-Qamdo-Gonjo region seems synchronous to the collision time around the EHS, but much earlier than those in the Lanping-Simao Terrane. In addition, the estimated shortening for the Eastern Tibetan Plateau is also not conclusive, ranging from ~ 1300 km (Tong et al., 2017) to ~ 600 km (van Hinsbergen et al., 2011a).

Given the above discordances on the time of deformation and amount of shortening, the tectonic evolution of the southeastern Tibetan Plateau is still not fully established. Here we present a new detailed paleomagnetic study of the Latest Eocene volcanic rocks in the Mangkang area, a region right in between the Nangqian-Qamdo-Gonjo and the Lanping-Simao basins (Fig. 1a). We first analyze the rotation pattern of the Mangkang Basin and its correlations to the adjacent basins, then estimate the amount of shortening during the Early Cenozoic, and finally discuss their tectonic significance.

2. Geological setting and paleomagnetic sampling

2.1. Geological setting

The southeastern Tibetan Plateau is composed of several elongated, fault-bounded terranes, including the Songpan-Ganzi,

Qiangtang, Lhasa, and Lanping-Simao-Indochina terranes. These terranes subsequently drifted away from Gondwana and accreted to Eurasia during late Paleozoic to early Cretaceous time, resulting in intervening suture zones (Guan et al., 2021; Metcalfe, 2013; Yan et al., 2016; Yin and Harrison, 2000; Yu et al., 2022). The tectonic feature in the region is characterized by a significant transition of strikes of the tectonic lineaments from E-W to N-S in the eastern Tibetan Plateau around the EHS (Fig. 1).

Our study area is located at Mangkang in the east part of the Qiangtang Terrane, which is bounded by the Jinshajiang Suture Zone to the east and the Bangong-Nujiang Suture Zone to the west. It lies on the north tip of the EHS where the faults and folds are gradually changing from NW-SE to N-S trending (Fig. 1a). Three unnamed small-scale strike-slip faults (F1, F2, F3) that cut through the Jurassic-Early Cenozoic strata are present in the region, with tens of kilometer left-lateral displacements (Fig. 1b).

The main sedimentary sequences in the Mangkang area are composed of the Upper Jurassic Xiali Fm. (mainly of sandstone and mudstone), the Lower Cretaceous Jingxing Fm., and the Upper Cretaceous Nanxin and Hutousi Fm. (mainly of sandstone and mudstone), which is in turn overlain by the Cenozoic Lawula Group (Fig. 2b). The Lawula Group is mainly composed of trachyte in the lower part and tuff, interbedded sandstone, and siltstone in the upper part, with a thickness of ~ 780 m in our study area (Fig. 2c; XGS, 2007; Ma et al., 2016; Su et al., 2018). This unit was previously assigned as Miocene in age (BGMRX, 1993), but was recently dated to be the Latest Eocene in age ($^{40}Ar/^{39}Ar$ and U/Pb ages of ~ 36.4–33.4 Ma for the trachyte and tuff layers) (Ma et al., 2016; Su et al., 2018). The Cretaceous strata in the Mangkang Basin were strongly folded, leading to steep beddings (mostly dip angles > 50°) in most areas or even overturned beddings in the margin of the basin (Fig. 2a, b). The Late Eocene Lawula Group was mildly tilted (mostly dips < 34°) and unconformably overlies the fierce-folded Cretaceous strata (Fig. 2a, b, e), with two limbs dipping northwest and southeast, respectively, yielding a NE-SW fold axis that is distinct to NW-SE fold axis of the Cretaceous red beds (Fig. 2a).

2.2. Paleomagnetic sampling

We sampled three localities near the Mangkang County, such as at Xuela (XL), Lawula (LW), and Lawula A (LWA) (Fig. 2a, 29.7°N, 98.6°E), which covers both the upper and lower part of Lawula Group. The Late-Eocene strata in locality XL are mainly composed of grayish-yellow tuff layers (Fig. 2d) that contain ~ 50% volcanic ash under microscopic thin sections (Fig. S1), with an identical bedding orientation (dip northwest, with dip angle of ~ 26°). A total of 4 horizons (sites) and 41 paleomagnetic samples were collected from ~ 40 m thick tuff layers by using a portable drill and oriented by both magnetic and sun compasses, where the intercalated sandstone and siltstone layers are too shattered to be sampled. (Fig. 2d). Locality LW is mainly composed of lava layers of trachyte that unconformably overlie the Upper Cretaceous Nanxin Fm (Fig. 2e). The bedding directions in the locality are not visible in the field but were assumed to be continuous to that of locality LWA, which is only 1 km away. A total of 10 sites and 101 paleomagnetic samples were oriented and collected. Locality LWA comprises gray and dark gray tuff layers (Fig. 2f, 2 g) that contain ~ 80% volcanic ash (Fig. S1), with clear beddings (dip southeast, with dip angle of ~ 34-50°), which are distinct from the tuff layers in XL (Fig. 2d). A total of 60 paleomagnetic samples were oriented and collected from 6 horizons (sites) in the ~ 50 m thick tuff layers. All core samples were cut into standard specimens with a length of 2.3 cm in the laboratory for rock magnetic and thermal demagnetization experiments.

3. Measurements and results

3.1. Rock magnetism

To investigate the magnetic properties of the samples, a total of ten representative samples were selected for detailed rock magnetic analyses. The results show almost identical for each locality, so only three specimens (XL2-10 for XL, LWA2-4 for LWA and LW1-1 for LW) were shown in Fig. 3. High-temperature magnetic susceptibility (χ-T) measurements were performed using an MFK1-FA Kappabridge and a CS-4 high-temperature furnace. Each sample was heated from room temperature to 700 °C and cooled back to room temperature in an argon atmosphere; hysteresis loops, isothermal remanent magnetization (IRM) acquisition with reverse field demagnetization curves and FORC diagrams were acquired using the Lakeshore 8604 Vibrating Sample Magnetometer. FORC diagrams were processed with FORCinel software (Harrison and Feinberg, 2008). All these rock magnetic analyses were conducted in the State Key Laboratory of Tibetan Plateau Earth System, Environment and Resources (TPESER) in the Institute of Tibetan Plateau, Chinese Academy of Sciences (ITPCAS).

The χ-T curves of samples XL2-10 and LWA2-4 show a dramatic decrease at ~ 580 °C to a very low intensity, followed by a slow decrease up to ~ 680 °C (Fig. 3a, 3b). In addition, χ peak of sample LWA2-4 is evident in the heating curve at ~ 300 °C but disappears in the cooling curve, which may be the result of a small amount of iron sulfide (e.g., pyrrhotite) that was transferred to magnetite during the subsequent heating process (Roberts et al., 2011). The IRM acquisition curve presents a sharp increase below 100 mT followed by a slow increase up to 1 T with low remanence coercivities (Bcr, ~29–38 mT; Fig. 3d, e), suggesting the low-coercivity magnetic components (e.g., magnetite) are dominant, with a small amount of high-coercivity magnetic components (e.g., hematite). Combined with χ-T curves of the above two samples, we deem that the major remanence carrier is magnetite, with a small amount of hematite and/or even pyrrhotite. This is consistent with the wasp-waisted hysteresis loops of sample XL2-10 (Fig. 3g), while sample LWA2-4 has a narrow hysteresis (Fig. 3h) that might be due to the higher proportion of magnetite relative to hematite. Sample LW1-1 shows a dramatic decrease in χ near ~ 580 °C and drops to nearly zero at ~ 600 °C, and a weak χ peak is evident in the heating curve at 300–400 °C (Fig. 3c), which may be the result of irreversible domain reorganization (Kosterov, 2001); its IRM acquisition and reverse field demagnetization curves reveal almost a fully saturation at 0.3 T, implying the major remanence carrier to be a "soft" magnetic phase, such as magnetite. This is further supported by the relatively narrow hysteresis loops and their low Bcr (~57 mT) (Fig. 3f, i). Additional insights by the FORC diagrams indicate that all the samples are pseudo-single-domain (PSD)-like. In summary, the above rock magnetic analyses suggest that the main magnetic carriers are PSD magnetite with few hematite, both of which could carry stable primary remanences.

3.2. SEM observation and EDS analysis

To reveal the morphology of the magnetic minerals that could estimate the reliability of the remanent magnetization, major element compositions of minerals for three representative samples of each locality were determined using a JEOL JXA-8230 electron probe micro-analyzer at the TPESER. Analyses were undertaken employing a 5 μm probe diameter size, for minerals with an accelerating voltage of 15 kV, beam current of 20 nA and 10 s counting times for peak and 5 s counting times for upper and lower background per element.

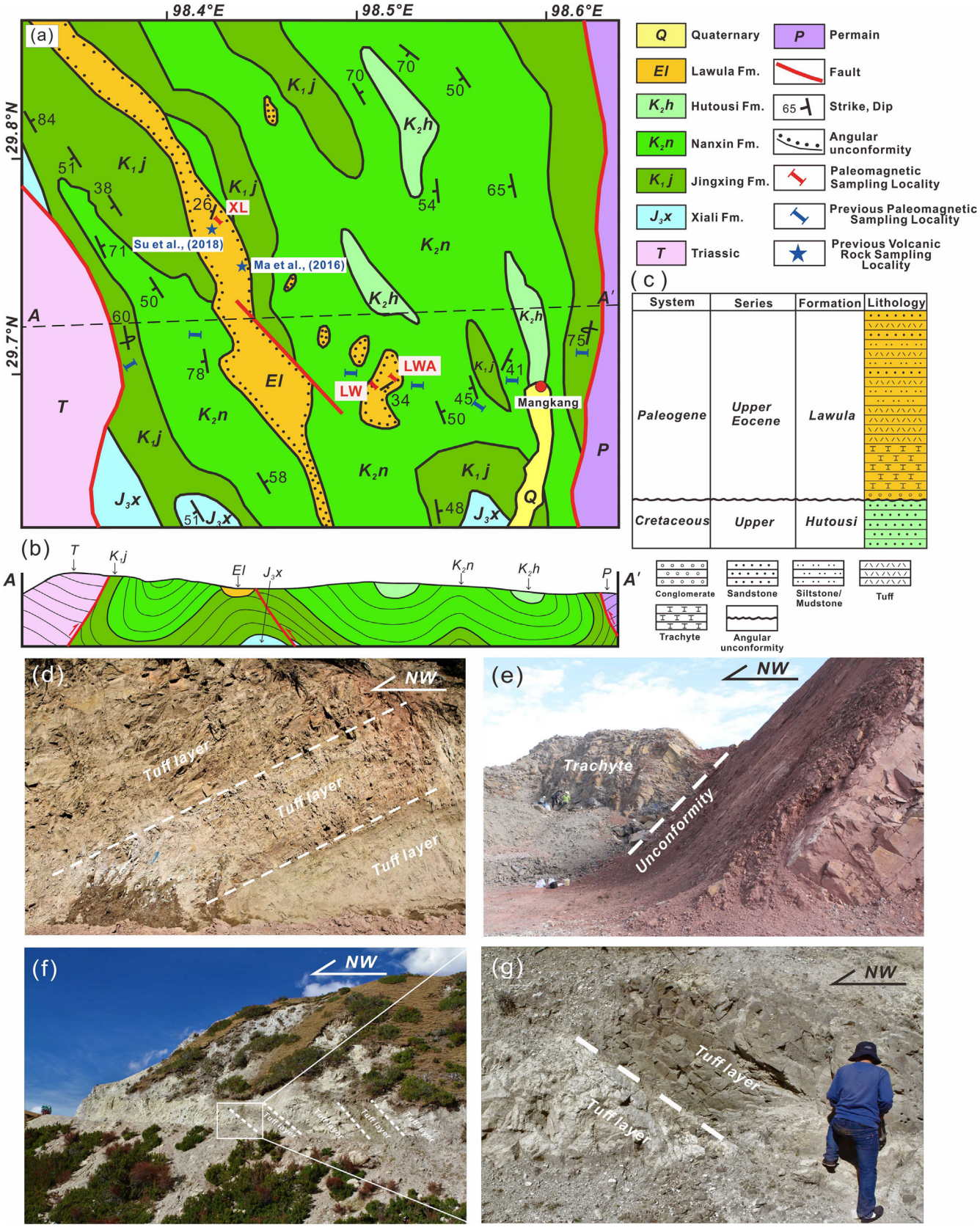

Fig. 2. (a) Simple geological map of the Mangkang area, showing the locations of the sampling localities and A-A' (modified from XGS, 2007); (b) Cross section of A-A'; (c) Lithologic sequence of the Cretaceous and Upper Eocene in the Mangkang area; (d) Representative lithology at locality XL, where the strata contain at least two tuff layers; (e) Angular unconformity between the Lawula and the Nanxin Formations at locality LW; (f, g) Representative lithology at locality LWA, where the strata contain at least 5 tuff layers.

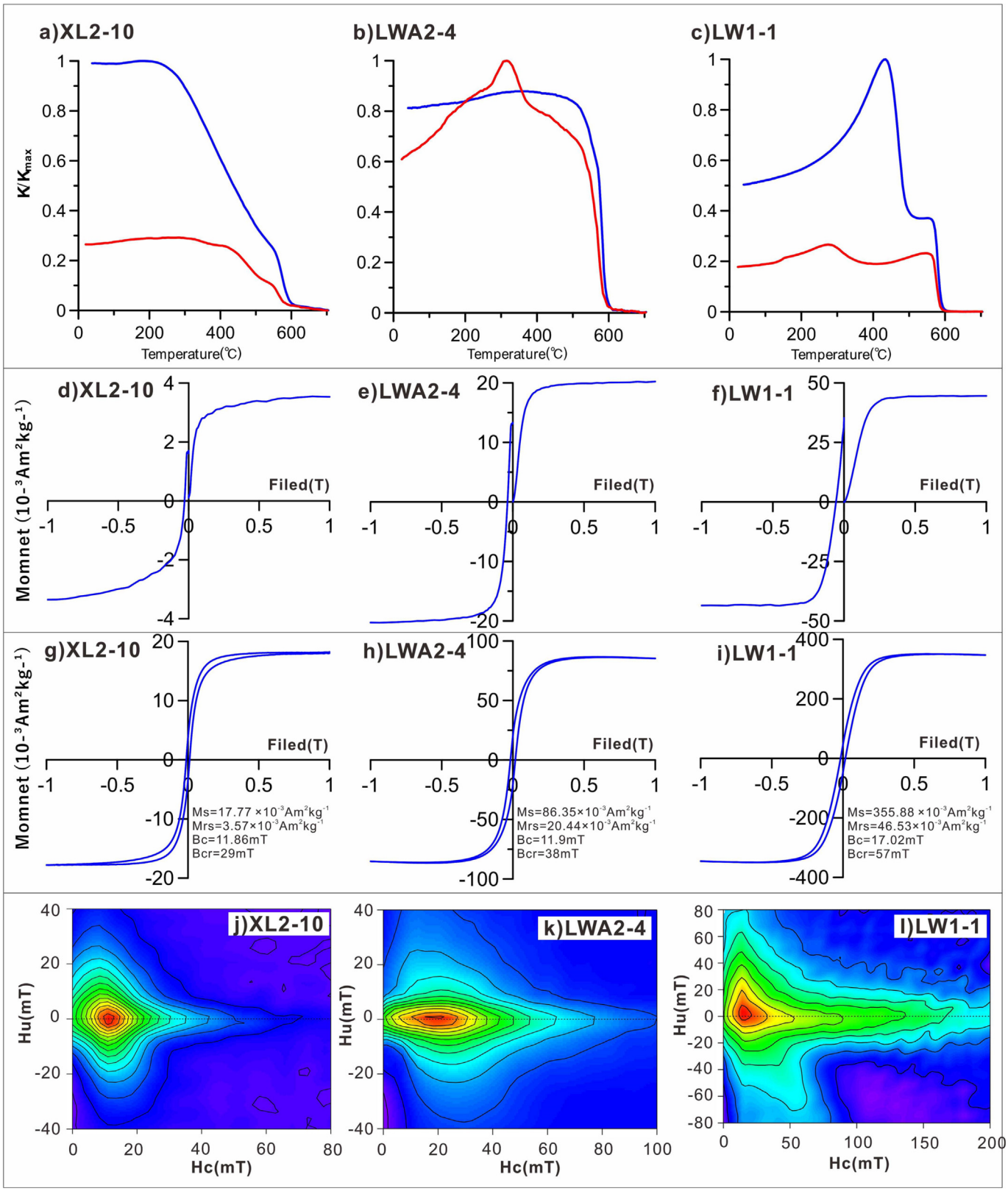

Fig. 3. High-temperature magnetic susceptibility curves (χ-T) (a-c), IRM acquisition curves with reverse-field demagnetization curves (d-f), Hysteresis loops (g-i, after slope correction) and FORC diagrams (j-l) for the three representative samples. The red (blue) lines denote heating (cooling) curves in (a-d). Ms, saturation magnetization; Mrs, saturation remanence; Bc, coercivity; Bcr, remanence coercive. (For interpretation of the references to colour in this figure legend, the reader is referred to the web version of this article.)

The observed iron oxides from these representative samples are prevailingly composed of Fe and O with idiographic particles containing Ti. These particles are mainly of magnetite with a small amount of hematite, based on rock magnetic investigations. The BSE images reveal that most iron oxide minerals are irregular in shape, range between 10 μm and 100 μm in size, and lack obviously oxidized rims. Solid-state exsolution characterized by a distribution of Ti-rich ilmenite in the Ti-poor magnetite is also scarce in our thin sections and only observed in idiographic magnetite grain (Fig. 4b), suggesting that most of the samples had experienced fast-ascent eruptions (Turner et al., 2008). All these results demonstrate that the observed iron oxides were likely formed during eruption without alteration, which can carry stable primary remnant magnetizations.

3.3. Paleomagnetic results

A total of 202 specimens were obtained and were all subjected to stepwise thermal demagnetizations using an ASC TD-48 oven (with a residual field < 10 nT) at intervals of 50–100 °C below 500 °C and 10–35 °C above 500 °C. The remanence was measured using a 2G-755 cryogenic magnetometer (RAPID system) in a magnetically shielded room with an average field intensity of ~ 170 nT in the paleomagnetic laboratory of TPESER. The thermal demagnetization result was plotted using the orthogonal diagram (Zijderveld, 1967) and the magnetization directions were determined by the principal component analyses (Kirschvink, 1980) using at least 4 subsequent steps. The site-mean directions were calculated using the Fisherian statistics (Fisher, 1953).

191 specimens contain low-temperature magnetic components (LTC) and can be isolated below ~ 300 °C (Fig. 5). Their in-situ mean direction is Dg = 7.8 ± 3.8°, Ig = 44.5 ± 4.3°, K = 9.9, A_{95} = 3.4°, which is close to the expected present-day geomagnetic field direction for the location (D = 0°, I = 48.8°). Their mean direction after tilt correction is Ds = 24.2 ± 8.1°, Is = 68.4 ± 3.5°, K = 5.1, A_{95} = 5°. The precision parameter (K) decreases from 9.9 to 5.1 after tilt correction and the eigenvalue (τ_1) reaches its maximum at 7–29 % unfolding in the Tauxe and Watson (1994) bootstrap fold test (Fig. 6a), suggesting that the LTC is post folding magnetization and most likely a recent viscous overprint. A total of 184 specimens contains high-temperature component (HTC) directions that can be isolated

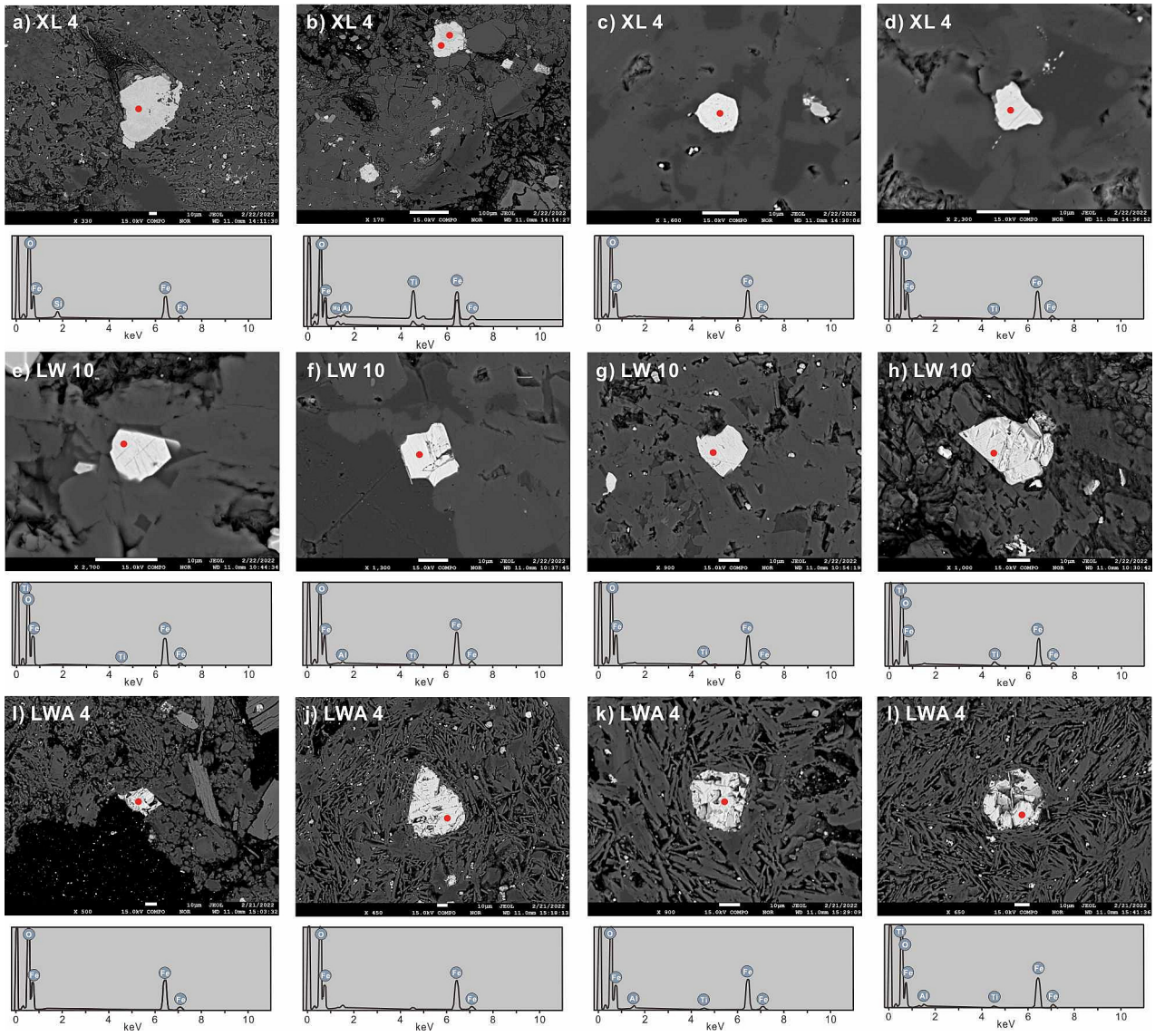

Fig. 4. Scanning electron microscopy backscatter electron (BSE) images and energy dispersive spectroscopy (EDS) images of the three representative samples. The red dots indicate the analyzed spots using EDS. (For interpretation of the references to colour in this figure legend, the reader is referred to the web version of this article.)

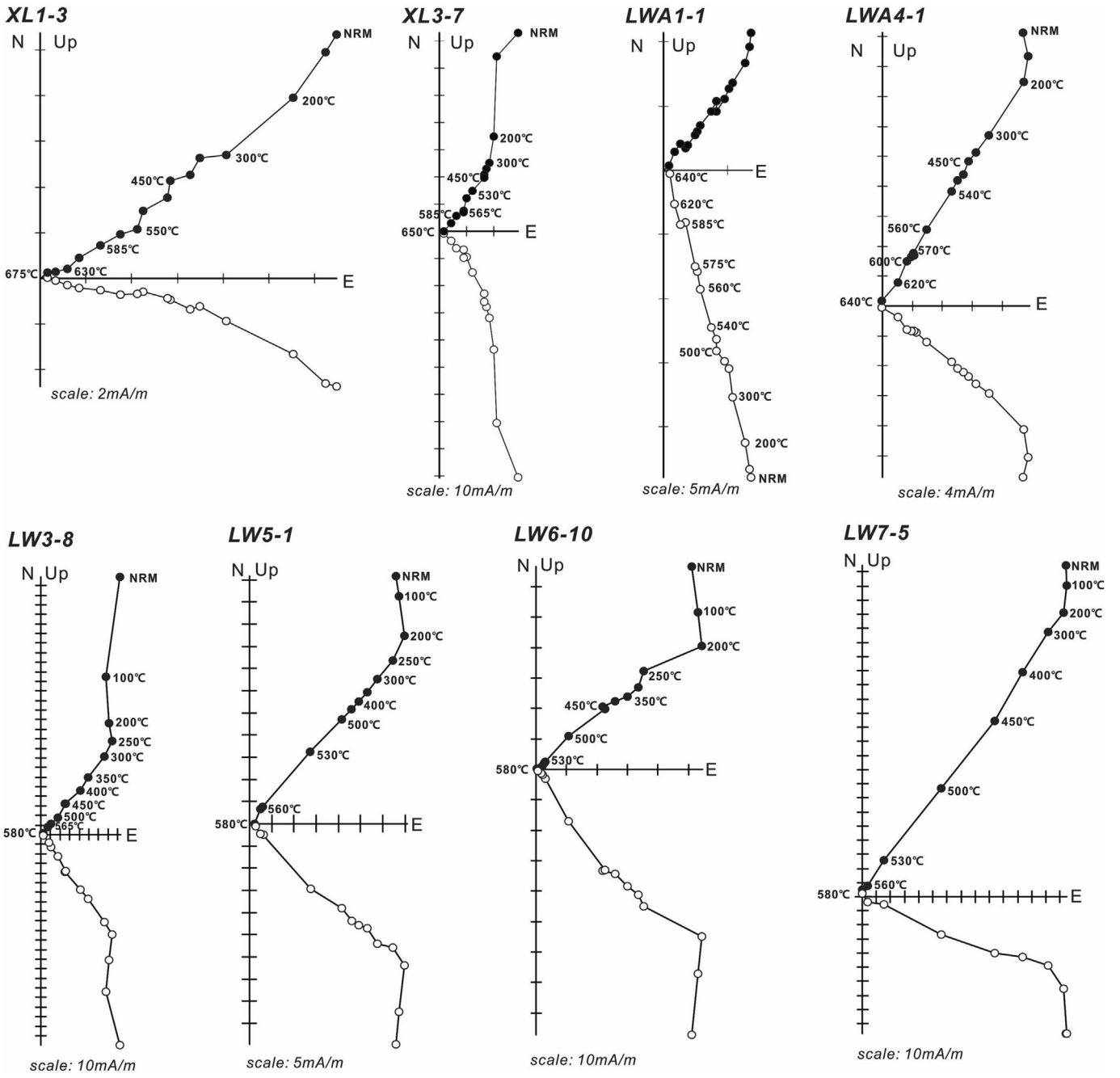

Fig. 5. Representative demagnetization diagrams for samples from the Mangkang area in geographic coordinate.

over 300 °C till up to 675 °C (Fig. 5), which mostly linearly decay to the origin and were interpreted as the characteristic remanent magnetizations (ChRMs). Meanwhile, the magnetization directions in magnetite and hematite are basically the same (Fig. 5).

The mean direction of 184 ChRMs is Dg = 43.4 ± 2.6°, Ig = 30.6 ± 4.0°, K = 19.0, A_{95} = 2.5° in-situ, and Ds = 62.6 ± 2.2°, Is = 46.7 ± 2.4°, K = 29.2, A_{95} = 2.0° after tilt correction. The highest value of τ1 is between 86 % and 102 % in the Tauxe and Watson (1994) progressive unfolding test (Fig. 6b), suggesting pre-folding magnetizations. The mean direction of the 20 sites is Dg = 44.3 ± 7.7°, Ig = 31.4 ± 11.7°, K = 20.7, A_{95} = 7.3° in-situ, and Ds = 62.2 ± 5.5°, Is = 47.6 ± 5.7°, K = 46.7, A_{95} = 4.8° after tilt correction (Table 1; Fig. 6c), which yield positive McFadden (1990) fold test both in 95 % and 99 % confidence levels (ξ1 = 8.23 before and ξ1 = 4.6 after tilt correction, with critical values of ξ = 5.21 at 95 % and ξ = 7.3 at 99 % confidence levels) and Tauxe and Watson (1994) progressive unfolding test (highest τ_1 between 80 % and 122 %) (Fig. 6c). Moreover, the possible influence of plunging fold was also checked, which indicate a mean direction of Ds'=65.2 ± 5.7°, Is'=47.7 ± 5.8°, K'=44.3, A_{95}'=4.9°. This mean direction is indistinguishable from the simple fold correction, but with a larger A_{95}. Thus, it seems insignificant plunging fold occurred within the studied section.

4. Discussion

4.1. Robustness of the paleomagnetic directions

The rock magnetic results, BSE observations, and EDS analyses have revealed that the magnetic carriers are mainly PSD magnetite

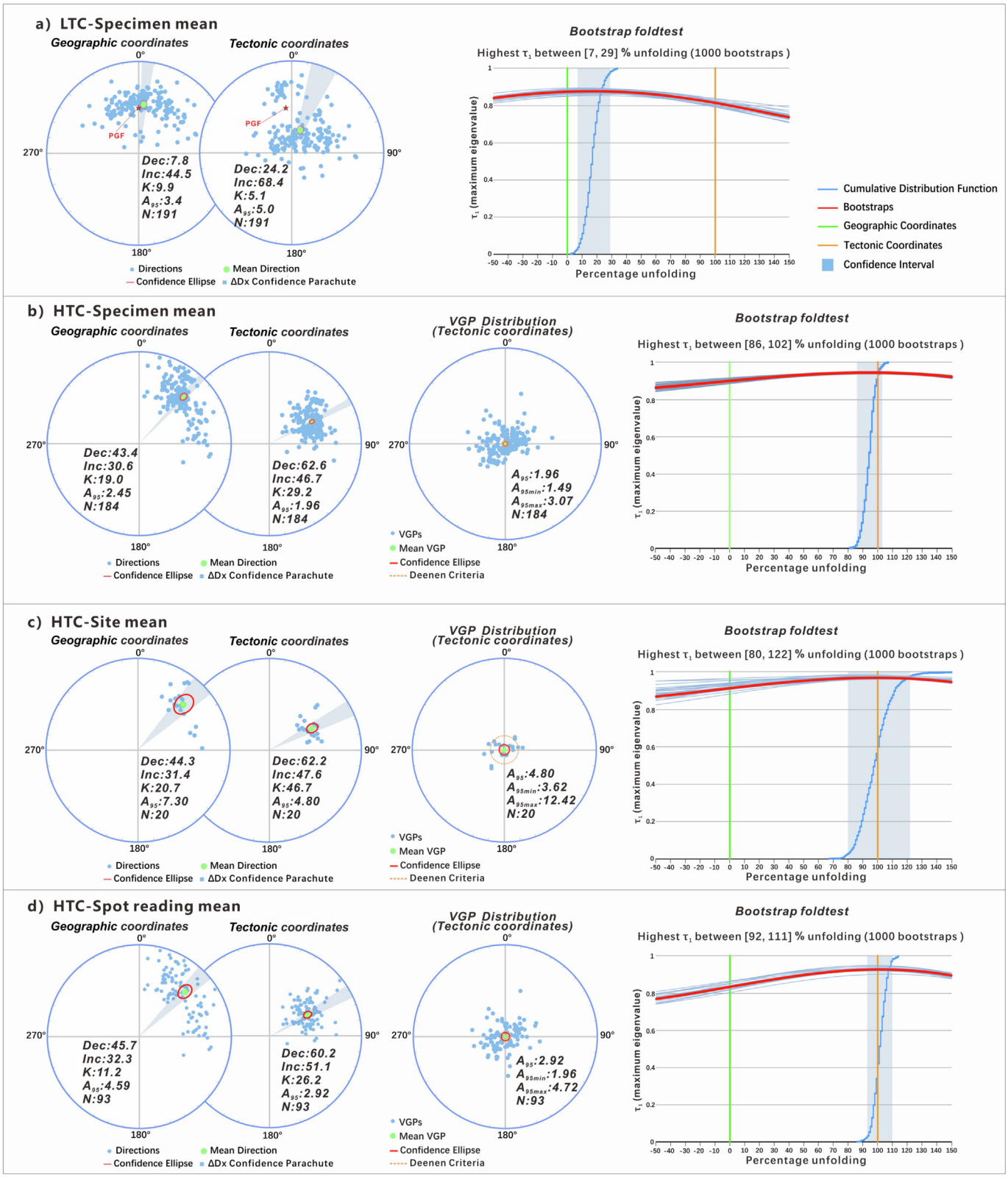

Fig. 6. Equal-area projections, plot of VGPs distributions and the Tauxe and Watson (1994) Fold test for the specimen means of LTC (a), and specimen means (b), the site means (c) and spot reading means of HTC (d). Note that all these mean directions are calculated by the online application paleomagnetism.org (Koymans et al., 2016, 2020).

and few hematite (Figs. 3, 4 and S1), which can carry stable remanence. No alteration is observed in the BSE and EDS images (Fig. 4), indicating likely of primary magnetizations. Detailed demagnetization analyses can easily separate two well-defined magnetic components in most samples (Fig. 5). The low-temperature components are likely of recent overprints. The HTCs are carried by magnetite and hematite, which are generally calculated above 300–350 °C and can avoid the possible interferences of pyrrhotite

Table 1
Paleomagnetic results of the Lawula Group in the Mangkang area.

Site ID	DD/Dip(°)	n/n0	Dg (°)	Ig (°)	Ds (°)	Is (°)	k	α_{95} (°)	A_{95} (°)	A_{95min}	A_{95max}
Xuela (29.8°N,98.4°E)											
XL 1	292/26	9/10	88.9	30.5	77.7	53.5	30.1	9.5	11.4	5.0	20.6
XL 2	292/26	9/10	68.6	32.6	50.5	48.9	34.2	8.9	9.4	5.0	20.6
XL 3	292/26	5/10	75.7	36.4	56.2	54.8	70.5	9.2	11.3	6.3	29.8
XL 4	292/26	7/11	72.1	39.9	48.7	56.5	45.3	9.1	10.6	5.5	24.1
Lawula A(29.7°N,98.5°E)											
LWA 1	165/34	6/8	33.6	35.8	64.1	51.7	24.6	13.8	13.2	5.9	26.5
LWA 2	165/34	11/11	38.0	44.3	78.4	55.1	47.6	6.7	7.3	4.6	18.1
LWA 3	165/34	10/11	24.3	36.8	55.6	57.5	44.7	7.3	8.5	4.8	19.2
LWA 4	165/34	9/10	36.3	31.3	62.4	45.7	78.6	5.9	5.2	5.0	20.5
LWA 5	170/50	9/9	26.5	21.2	59.7	53.8	61.8	6.6	8.4	5.0	20.5
LWA 6	170/50	8/11	22.5	10.0	42.8	48.4	73.9	6.5	7.0	5.2	22.1
Lawula(29.7°N,98.5°E)											
LW 1	165/34	10/10	41.0	27.5	63.2	41.3	291.4	2.8	3.0	4.8	19.2
LW 2	165/34	11/11	37.6	27.2	59.8	42.9	491.3	2.1	2.4	4.6	18.1
LW 3	165/34	10/10	41.7	36.3	72.0	47.6	550.5	2.1	2.4	4.8	19.2
LW 4	165/34	10/10	52.1	36.5	80.6	41.9	278.8	2.9	2.3	4.8	19.2
LW 5	165/34	11/11	38.9	36.7	69.9	49.5	202.5	3.2	3.4	4.6	18.1
LW 6	165/34	10/10	44.2	33.3	71.2	44.0	110.9	4.6	4.6	4.8	19.2
LW 7	165/34	10/10	41.5	27.6	63.8	41.1	178.2	3.6	3.7	4.8	19.2
LW 8	165/34	10/10	35.1	12.7	47.1	32.2	830.0	1.7	1.4	4.8	19.2
LW 9	165/34	9/9	36.3	10.1	46.8	29.3	297.6	3.0	3.1	5.0	20.5
LW 10	165/34	10/10	47.2	36.6	76.9	44.8	33.0	8.5	9.1	4.8	19.2
Mean		**20/20**	**44.3**	**31.4**			**20.3**	**7.4**			
		20/20			**62.2**	**47.6**	**60.7**	**4.2**			

Note: Site ID, paleomagnetic site identification; DD/Dip, Dip direction and Dip of the bed; n/n0, number of samples used to calculate the mean/demagnetized; Dg, Ig (Ds, Is), declination and inclination before (after) tilt correction; k, precision parameter; α_{95}, radius of the circle of 95 % confidence. Noted that samples of localities XL and LWA were from multiple tuff layers, while those of locality LW were from lava units.

(unblocking temperature at 270 °C for monoclinic system or 325 °C for hexagonal system) in some of the samples. The obtained 184 ChRMs of 20 sites yield pre-folding magnetizations (Fig. 6b-d). The time of folding in the Mangkang area was not well documented, due to limited exposure of the Cenozoic strata, we could only discreetly infer the folding of the Lawula Group to post-Eocene by the eruption age of the Lawula Group, which is not helpful. But all the other lines of evidence above suggest primary magnetizations of the ChRMs. Meanwhile, as mentioned, the bedding directions of LW locality are invisible in the field and were assigned to that of the nearby locality LWA. There was no observable local fault in-between the two localities (Fig. 2a), and the site-average directions of the two localities are indistinguishable from each other (Ds = 65.1 ± 12.6°, Is = 52.8 ± 11°, K = 78.1, A_{95} = 10.5° for LW and Ds = 64.4 ± 7.6°, Is = 42 ± 7.6°, K = 50, A_{95} = 6.9° for LWA). It is thus likely indicating a reasonable assignment for the bedding directions of Locality LW.

It is important when sampling volcanic rocks to ascertain whether the distribution of the paleomagnetic data has sufficiently well-sampled paleosecular variation (PSV) or still a spot reading. In our case, we sampled lavas and tuffs. The lavas tend to have higher k-values ($\gg$50) than the tuffs (20–30) (Table 1). When A_{95} values are computed from the tuff horizons, they fall within the Deenen et al. (2011) envelope, and on this basis alone, it would be possible that each tuff sample represents a spot reading. Assuming that, we may compute an average direction based on N = 93 directions of Ds = 60.2 ± 3.4°, Is = 51.1 ± 3.2°, K = 26.2, A_{95} = 2.9°, which would fall within the A_{95}min, max envelope for N = 93 (2.0, 4.7°) (Deenen et al., 2011), yielding a positive McFadden (1990) fold test both in 95 % and 99 % confidence levels (ξ1 = 52.6 before and ξ1 = 9.2 after tilt correction, with critical values of ξ = 11.4 at 95 % and ξ = 16.1 at 99 % confidence levels) and a Tauxe and Watson (1994) progressive unfolding test (highest τ1 between 92 % and 111 %) (Fig. 6d). However, tuffs form during eruptions, and the narrow stratigraphic ranges that we sampled per 'site' should have formed geologically instantaneously. In that case, the lower k-values of the tuff sites may indicate more spurious magnetizations and assuming that each tuff sample represents a spot reading is geologically unlikely could bias the pole towards the lowest-quality data. Treating each volcanic horizon as a spot reading would lead to an N = 20 average of Ds = 62.2 ± 5.5°, Is = 47.6 ± 5.7°, K = 46.7, A_{95} = 4.8°. This is statistically indistinguishable from the N-93 pole, also passes the Deenen et al. (2011) criteria (N = 20 (3.6, 12.4°)), and is the more conservative estimate. For our tectonic interpretation, the two approaches give the same result.

Both the tuff layers and trachyte were sampled from the upper and lower part of the Lawula Group. The sampled ~ 40 m tuff sequence in locality XL was previously Ar-Ar dated to be 33.4–35.5 Ma (Su et al., 2018), and the sampled trachyte layer in locality LW was previously U/Pb dated to be 35.2–36.4 Ma (Ma et al., 2016). A time scale of 10^4-10^5 yr is usually enough to meet a geocentric axial dipole (GAD) model (Johnson et al., 2008), so that the duration of ~ 3 Ma in this study is long enough to represent a PSV averaged field. Thus, our obtained mean paleomagnetic direction and the pole are representative for the time-averaged Latest Eocene magnetic field of the Mangkang area.

In summary, both the robust and PSV analyses indicate that the obtained new paleomagnetic directions (Ds = 62.2 ± 5.5°, Is = 47.6 ± 5.7°, K = 46.7, A_{95} = 4.8°) from the upper and lower part of the Lawula Group are primary magnetizations and their mean can represent a reliable Latest Eocene (~33.4–36.4 Ma) Earth magnetic field.

4.2. Post-Eocene significant clockwise rotation and its tectonic implications

The conventional way of calculating rotation is comparing the paleomagnetic pole to the reference pole centered on the given age (e.g. 50 Ma, 60 Ma, or 70 Ma) (Torsvik et al., 2012). Recently, Vaes et al. (2023) proposed a new method to calculate the apparent polar wander path based on site-level paleomagnetic data with an updated paleomagnetic database and relative plate motion model, which could incorporate both spatial and temporal uncertainties of the original datasets. This new method allows us to compute the

reference pole for any given age range (Table S1). In addition, Vaes et al. (2022) showed that to obtain a 95 % certainty that a difference between a study pole and a reference pole is geologically meaningful requires weighting the uncertainty of the reference pole against the number of sites (i.e. paleomagnetic spot readings) of the study mean (their 'B_{95}'). Using this metric, the Mangkang area has experienced a significant clockwise rotation relative to Eurasia of 53.0 ± 8.0° after 34.9 ± 1.5 Ma. Three other paleomagnetic studies that were conducted on the Cretaceous red beds around the study area (Table S1), which revealed 30.3 ± 13.1° or 42.0 ± 10.6° clockwise rotation relative to Eurasia after the Early Cretaceous (Huang et al., 1992; Otofuji et al., 1990), and 27.4 ± 14.7° or 43.6 ± 14° clockwise rotation relative to Eurasia after the Late Cretaceous (Huang et al., 1992; Tong et al., 2015). A compilation of the three studies indicates a significant clockwise rotation of 37.2 ± 8.2° after the Early Cretaceous or 38.7 ± 10.7° after the Late Cretaceous relative to Eurasia (Tong et al., 2015). All these together indicate that the Mangkang Basin has experienced significant clockwise rotation since the Late Eocene (i.e., 36–33 Ma). But the magnitudes of clockwise rotation from the Cretaceous sequences (Huang et al., 1992; Otofuji et al., 1990; Tong et al., 2015) are slightly less than that of this study, suggesting slight (~15°) counterclockwise rotation relative to Eurasia of the Mangkang area between the Cretaceous and the Late Eocene (~36–33 Ma) (Table S1).

To better understand the rotations observed in the Mangkang area, we integrated other available paleomagnetic results from the adjacent basins. For example, three paleomagnetic studies have been carried out on the thick Early Cenozoic red bed sequences of the Gonjo Basin (Li et al., 2020; Studnicki-Gizbert et al., 2008), which is ~ 100 km north of Mangkang. A paleomagnetic study on the Eocene red beds in the Gonjo Basin revealed a significant clockwise rotation of ~ 24.6 ± 7.4° relative to Eurasia after 43.2 Ma (Tong et al., 2017). A subsequent study revealed upward decreasing declinations, and 17.7 ± 3.3° clockwise rotation after 43 Ma in the Gonjo Basin (Zhang et al., 2018). The detailed magnetostratigraphy-based rotation analysis showed a ~ 10° counterclockwise rotation during 69–67 Ma followed by ~ 30° clockwise rotation during 52–48 Ma and another ~ 23.9 ± 11° clockwise rotation relative to Eurasia after 41 Ma (Li et al., 2020). The above studies indicate a significant clockwise rotation of ~ 20° relative to Eurasia after 41 Ma for the Gonjo Basin, though discordant rotations existed before 41 Ma. Thus, both significant post-Eocene clockwise were observed in the Gonjo and the Mangkang Basins, where the former is considerably (~30°) less than that in the Mangkang Basin. This large-scale difference in rotation between the Mangkang and Gonjo Basin is not readily explained by statistical properties of the magnetic field (e.g., Vaes et al., 2022), but requires a tectonic cause.

The strikes of the main faults and fold axis of the Jurassic-Cretaceous strata around the Gonjo-Mangkang region change slightly from north to south (Fig. 7a), such as NW-SE in the Gonjo Basin, N-S in the Mangkang Basin. The calculated mean strike of the faults and fold axis strike is ~ 140°SE in the Gonjo Basin and ~ 170°SE in the Mangkang Basin (Fig. 7b), showing signs of a small-scale bending in this area, with an integrated magnitude of ~ 30°, which is consistent to that of the rotation recorded by paleomagnetism. In addition, there also exist three small-scale left-lateral strike-slip faults in between the Gonjo and Mangkang basins, which are recognizable by the displacements of the Proterozoic-Cenozoic strata (Fault 1, 2 and 3 in Fig. 1b and 7a; Studnicki-Gizbert et al., 2008). Meanwhile, Faults 2 and 3 cut through the lower Tertiary stratigraphy (~69–41 Ma, Li et al., 2020; Studnicki-Gizbert et al., 2008; Tang et al., 2017), yielding post-Eocene activities. The activities of these three faults may also indicate that they have adjusted the differential rotations between the Gonjo and Mangkang basins. We therefore postulate that the additional 30° clockwise rotation in the Mangkang Basin after the Latest Eocene is the result of more intense E-W shortening in the wide shear zone than the Gonjo Basin, thus, a small-scale oroclinal bending in the Gonjo and Mangkang area around the EHS (Fig. 7c). Consequently, both the geological evidence and the magnitude coincidence in the paleomagnetic rotation and strike differences indicate the deformation in the Gonjo-Mangkang Basins was likely in an oroclinal bending fashion around the EHS, such as also suggested by some studies (Deng et al., 2020; Todrani et al., 2021; van Hinsbergen et al., 2011b; Zhang et al., 2020).

In addition, we are aware of the existence of a slight counterclockwise rotation between the Late Cretaceous and the Late Eocene in the Mangkang Basin (Table S1). Although the mechanism and time of rotation are still not clear, we simply deemed its location around the west side of the tip of the EHS during sometime between the Late Cretaceous and the late Eocene that might be the cause of the counterclockwise rotation, akin to that of the Nangqian Basin during the early Eocene (Zhang et al., 2020). More studies are required to provide further insights into the deformation models and mechanisms.

4.3. Implications on the Cenozoic crustal shortening in the eastern Tibetan Plateau

Volcanic rocks are likely immune to inclination shallowing bias and are rather robust for paleolatitude constraint. Our obtained paleomagnetic pole is 36.4°N, 173.1°E, with A_{95} = 4.8° for the latest Eocene (33.4–36.4 Ma) Mangkang Basin (site at 29.7°N, 98.6°E), yielding a paleolatitude of 28.7 ± 4.8°N. The reference pole of Eurasia is 82°N, 181.5°E, with B_{95} = 7.2° centered at 34.9 Ma (the middle age of Lawula volcanic rocks) in 10 Ma time window (Vaes et al., 2023), indicating 1.9 ± 6.9°, or 211 ± 766 km latitudinal crustal convergence between the Eurasian and eastern Qiangtang since the Late Eocene.

Recently, Tong et al. (2017) reported an E/I corrected red bed paleolatitude of 23.9 ± 2.9°N during 56–43.2 Ma in Gonjo Basin, which is consistent with the "Class A" E/I corrected paleolatitude of 23.2 ± 3.6°N during 49–50.6 Ma (Vaes et al., 2021). Compared with the Eurasian reference poles centered at the middle age of these two datasets, the latitudinal differences between the expected and observed paleolatitudes are 12.0 ± 6.1° and 12.4 ± 5.9°, or 1332 ± 677 km and 1376 ± 655 km (Table S1). Given the amount of 211 ± 766 km latitudinal difference between the expected and observed paleolatitude at the latest Eocene in Mangkang Basin, it indicates that the area between Eurasian and eastern Qiangtang has experienced latitudinal convergence with Eurasia during the Middle-Late Eocene. The angular unconformably overlain of the highly folded Cretaceous strata by the slightly tilted latest Eocene Lawula Group also supports significant deformations during this period (Fig. 2b). The widely existing folding and thrusting in the Mangkang Basin indicates ~ 40 % (~40 km) upper crustal shortening by the balance cross section (Fig. 2b), akin to the shortening rate estimated in the Yushu-Nangqian fold-thrust belt (Spurlin et al., 2005) (Fig. 1a).

The convergence estimated by paleomagnetic results is consistent with the shortening history of eastern Tibet of ~ 1200 km in the last 50 Ma reconstructed from shortening and strike-slip estimates and vertical axis rotations (van Hinsbergen et al., 2019). In addition, significant late Eocene uplifts have been reported for the Gonjo-Mangkang region (Su et al., 2018; Tang et al., 2017; Xiong et al., 2020), the uplift from a low land to a high plateau might have also consumed significant crustal shortening (e.g., Song et al., 2022). All these together suggested the likelihood of > 1000 km crustal shortening, just like the paleomagnetic results

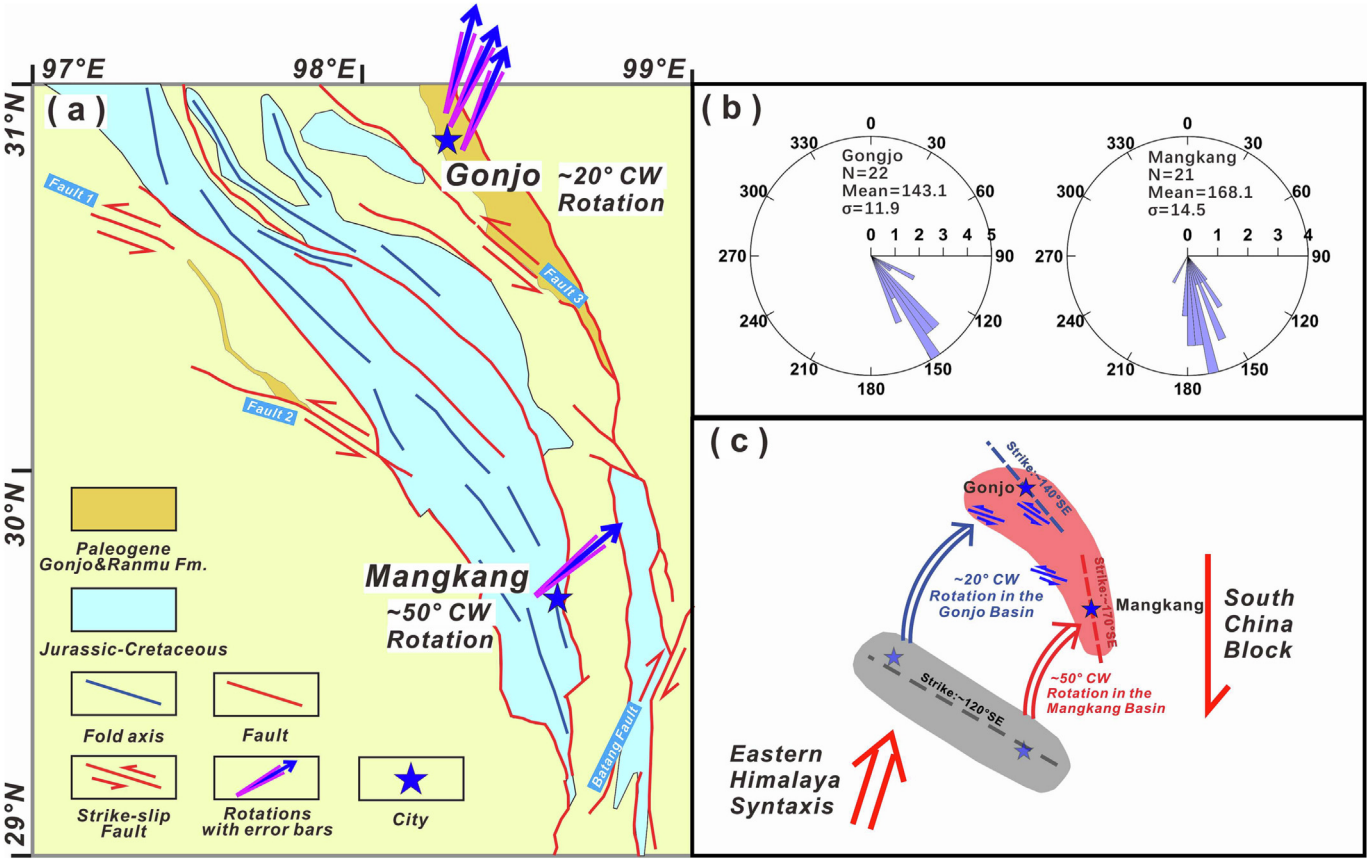

Fig. 7. (a) Sketch map showing the main fault and fold axes of the Gonjo-Mangkang area. The blue area is the roughly shape of the Jurassic-Cretaceous strata in Fig. 7a; (b) Directional statistics of the main faults and fold axes in the Gonjo-Mangkang area; (c) Cartoon showing different post-Late Eocene rotations in the Mangkang and Gonjo basins. The grey shadow and grey line represent the pre-rotation shape and strike, where the red shadow represent the present shape of the Gonjo-Mangkang region, and the blue and red lines are the present strike of Gonjo and Mangkang separately. (For interpretation of the references to colour in this figure legend, the reader is referred to the web version of this article.)

have revealed, in the area between Eurasian and eastern Qiangtang during the Cenozoic.

5. Conclusion

Detailed SEM and EDS, rock magnetic, and paleomagnetic analyses of the Latest Eocene volcanic rocks revealed a primary magnetic direction of Ds = 62.2 ± 5.5°, Is = 47.6 ± 5.7°, K = 46.7, A_{95} = 4.8° for the Mangkang Basin. The new paleomagnetic result revealed a ~ 50° clockwise rotation of the Mangkang Basin with respect to Eurasian after 36–33 Ma. By analyzing the spatial and temporal variations in paleomagnetic rotations and fault-fold-strata strikes of the Gonjo-Mangkang region, we speculated that the clockwise rotation in the Gonjo-Mangkang area is a result of oroclinal bending around the EHS. The robust Latest Eocene volcanic inclination in the Mangkang Basin and the corrected inclination in the Gonjo Basin suggest extensive Eocene crustal shortening which is consistent with geological estimations.

CRediT authorship contribution statement

Wanlong Xu: Conceptualization, Methodology, Formal analysis, Investigation, Writing – original draft, Visualization. **Maodu Yan:** Conceptualization, Methodology, Investigation, Writing – review & editing, Supervision, Funding acquisition. **Douwe J.J. van Hinsbergen:** Conceptualization, Methodology, Investigation, Writing – review & editing. **Bingshuai Li:** Formal analysis, Investigation. **Chong Guan:** Formal analysis, Investigation. **Qiang Fu:** Formal analysis, Investigation. **Liang Yu:** Formal analysis, Investigation. **Zunbo Xu:** Formal analysis, Investigation. **Dawen Zhang:** Formal analysis, Investigation. **Miaomiao Shen:** Formal analysis, Investigation. **Zhantao Feng:** Formal analysis, Investigation. **Zhichao Niu:** Formal analysis, Investigation. **Bram Vaes:** Methodology, Formal analysis.

Declaration of competing interest

The authors declare that they have no known competing financial interests or personal relationships that could have appeared to influence the work reported in this paper.

Acknowledgments

This work is co-supported by the National Natural Science Foundation of China (Grants 41974080, 41988101-01), the National Key Research and Development Program of China (2022YFF0800502), the Second Tibetan Plateau Scientific Expedition and Research Grant (2019QZKK0707), and China Scholarship Council. We thank Yuwei Zhang, and Jing Xie for laboratory assistance. Data in this paper are available online https://data.tpdc.ac.cn/en/disallow/d745ff4c-d1c5-4716-b6f7-5c22652d338d) and will be made available in the Paleomagnetism.org and MagIC databases. Finally, we sincerely thank the Associate Editor Joseph G. Meert, Daniel Pastor-Galán and another anonymous reviewer for their insightful comments and suggestions that greatly improved this paper.

Appendix A. Supplementary material

Supplementary data to this article can be found online at https://doi.org/10.1016/j.gr.2023.12.004.

References

Baral, U., Ding, L., Goswami, T.K., Sarma, M., Qasim, M., Bezbaruah, D., 2019. Detrital zircon U-Pb geochronology of a Cenozoic foreland basin in Northeast India: Implications for zircon provenance during the collision of the Indian and Asian plates. Terra Nova 31, 18–27.

BGMRX (Bureau of Geology Mineral Resources of Xizang Autonomous Region), 1993, Regional geology of Xizang (Tibet) autonomous region, (p. 515). Beijing: Geological Publishing House. (In Chinese).

Chung, S.L., Lee, T.Y., Lo, C.H., Wang, P.L., Chen, C.Y., Yem, N.T., Hoa, T.T., Wu, G.Y., 1997. Intraplate extension prior to continental extrusion along the Ailao Shan Red River shear zone. Geology 25, 311–314.

Deenen, M.H.L., Langereis, C.G., van Hinsbergen, D.J.J., Biggin, A.J., 2011. Geomagnetic secular variation and the statistics of palaeomagnetic directions. Geophys. J. Int. 186, 509–520.

Deng, J., Wang, Q., Gao, L., He, W., Yang, Z., Zhang, S., Chang, L., Li, G., Sun, X., Zhou, D., 2020. Differential crustal rotation and its control on giant ore clusters along the eastern margin of Tibet. Geology 49, 428–432.

Fang, X.M., Dupont-Nivet, G., Wang, C.S., Song, C.H., Meng, Q.Q., Zhang, W.L., Nie, J.S., Zhang, T., Mao, Z.Q., Chen, Y., 2020. Revised chronology of central Tibet uplift (Lunpola Basin). Sci. Adv. 6, 1–10.

Fisher, R., 1953. Dispersion on a sphere. Proc. R. Soc. A: Math. Phys. Eng. Sci. 217, 295–305.

Gao, L., Yang, Z.Y., Tong, Y.B., Wang, H., An, C.Z., 2015. New paleomagnetic studies of Cretaceous and Miocene rocks from Jinggu, western Yunnan, China: evidence for internal deformation of the Lanping-Simao Terrane. J. Geodyn. 89, 39–59.

Guan, C., Yan, M.D., Zhang, W.L., Zhang, D.W., Fu, Q., Yu, L., Xu, W.L., Zan, J.B., Li, B.S., Zhang, T., Shen, M.M., 2021. Paleomagnetic and Chronologic Data Bearing on the Permian/Triassic Boundary Position of Qamdo in the Eastern Qiantang Terrane: Implications for the Closure of the Paleo-Tethys. Geophys. Res. Lett. 48, 1–10.

Hall, R., 2002. Cenozoic geological and plate tectonic evolution of SE Asia and the SW Pacific: computer-based reconstructions, model and animations. J. Asian Earth Sci. 20, 353–431.

Harrison, R.J., Feinberg, J.M., 2008. FORCinel: An improved algorithm for calculating first-order reversal curve distributions using locally weighted regression smoothing. Geochem. Geophys. Geosyst. 9, 1–11.

Harrison, T.M., Leloup, P.H., Ryerson, F.J., Tapponnier, P., Lacassin, R., Chen, W., 1996. Diachronous initiation of transtension along the Ailao Shan-Red River Shear zone, Yunnan and Vietnam. In: Yin, A., Harrison, T.M. (Eds.), The Tectonic Evolution of Asia. Cambridge University Press, New York, pp. 208–226.

He, X.H., Tan, S.C., Zhou, J.X., Liu, Z., Zhao, Z.F., Yang, S.Q., Zhang, Y.H., 2020. Identifying the leucogranites in the Ailaoshan-Red River shear zone: Constraints on the timing of the southeastward expansion of the Tibetan Plateau. Geosci. Front. 11, 765–781.

Huang, K.N., Opdyke, N.D., Li, J., Peng, X., 1992. Paleomagnetism of Cretaceous rocks from Eastern Qiangtang Terrane of Tibet. J. Geophys. Res. Solid Earth 97, 1789–1799.

Johnson, C.L., Constable, C.G., Tauxe, L., Barendregt, R., Brown, L.L., Coe, R.S., Layer, P., Mejia, V., Opdyke, N.D., Singer, B.S., Staudigel, H., Stone, D.B., 2008. Recent investigations of the 0–5 Ma geomagnetic field recorded by lava flows. Geochem. Geophys. Geosyst. 9, 1–31.

Kirschvink, J.L., 1980. The least-squares line and plane and the analysis of paleomagnetic data. Geophys. J. R. Astron. Soc. 62, 699–718.

Kosterov, A., 2001. Magnetic properties of subaerial basalts at low temperatures. Earth Planets Space 53, 883–892.

Koymans, M.R., Langereis, C.G., Pastor-Galán, D., van Hinsbergen, D.J.J., 2016. Paleomagnetism.org: An online multi-platform open source environment for paleomagnetic data analysis. Comput. Geosci. 93, 127–137.

Koymans, M.R., van Hinsbergen, D.J.J., Pastor-Galán, D., Vaes, B., Langereis, C.G., 2020. Towards FAIR Paleomagnetic Data Management Through Paleomagnetism.org 2.0. Geochem. Geophys. Geosyst. 21, 1–7.

Leloup, P.H., Lacassin, R., Tapponnier, P., Scharer, U., Zhong, D.L., Liu, X.H., Zhang, L. S., Ji, S.C., Trinh, P.T., 1995. The Ailao Shan-Red River shear zone (Yunnan, China), Tertiary transform boundary of Indochina. Tectonophysics 251, 3–84.

Leloup, P.H., Arnaud, N., Lacassin, R., Kienast, J.R., Harrison, T.M., Trong, T.T.P., Replumaz, A., Tapponnier, P., 2001. New constraints on the structure, thermochronology, and timing of the Ailao Shan-Red River shear zone, SE Asia. J. Geophys. Res. Solid Earth 106, 6683–6732.

Li, S.H., Advokaat, E.L., van Hinsbergen, D.J.J., Koymans, M., Deng, C., Zhu, R., 2017a. Paleomagnetic constraints on the Mesozoic-Cenozoic paleolatitudinal and rotational history of Indochina and South China: Review and updated kinematic reconstruction. Earth Sci. Rev. 171, 58–77.

Li, S.H., Yang, Z.Y., Deng, C.L., He, H.Y., Qin, H.F., Sun, L., Yuan, J., van Hinsbergen, D.J. J., Krijgsman, W., Dekkers, M.J., Pan, Y.X., Zhu, R.X., 2017b. Clockwise rotations recorded in redbeds from the Jinggu Basin of northwestern Indochina. Geol. Soc. Am. Bull. 129, 1100–1122.

Li, S.H., van Hinsbergen, D.J.J., Najman, Y., Liu-Zeng, J., Deng, C., Zhu, R., 2020. Does pulsed Tibetan deformation correlate with Indian plate motion changes? Earth Planet. Sci. Lett. 536, 116144.

Ma, H.J., Zhang, S.T., Lin, N., Cheng, X.F., Zhang, L., 2016. LA-ICP-MS zircon U-Pb dating of the trachyte and its significance in Mangkang basin. Tibet. Sci. Technolo. Eng. 16, 1671–1815. in Chinese with English abstract.

Mazur, S., Green, C., Stewart, M.G., Whittaker, J.M., Williams, S., Bouatmani, R., 2012. Displacement along the Red River Fault constrained by extension estimates and plate reconstructions. Tectonics 31, TC5008.

McFadden, P.L., 1990. A new fold test for palaeomagnetic studies. Geophys. J. Int. 103, 163–169.

Metcalfe, I., 2013. Gondwana dispersion and Asian accretion: Tectonic and palaeogeographic evolution of eastern Tethys. J. Asian Earth Sci. 66, 1–33.

Molnar, P., England, P., 1990. Late Cenozoic Uplift of Mountain-Ranges and Global Climate Change - Chicken or Egg. Nature 346, 29–34.

Otofuji, Y., Inoue, Y., Funahara, S., Murata, F., Zheng, X., 1990. Paleomagnetic study of eastern Tibet-deformation of the Three Rivers region. Geophys. J. Int. 103, 85–94.

Replumaz, A., Tapponnier, P., 2003. Reconstruction of the deformed collision zone between India and Asia by backward motion of lithospheric blocks. J Geophys. Res. Solid Earth 108 (B6), 2285.

Roberts, A.P., Chang, L., Rowan, C.J., Horng, C.-S., Florindo, F., 2011. Magnetic properties of sedimentary greigite (Fe3S4): An update. Rev, Geophys, p. 49.

Royden, L.H., Burchfiel, B.C., van der Hilst, R.D., 2008. The geological evolution of the Tibetan Plateau. Science 321, 1054–1058.

Sato, K., Liu, Y.Y., Zhu, Z.C., Yang, Z.Y., Otofuji, Y., 1999. Paleomagnetic study of middle Cretaceous rocks from Yunlong, western Yunnan, China: evidence of southward displacement of Indochina. Earth Planet. Sci. Lett. 165, 1–15.

Searle, M.P., 2006. Role of the Red River Shear zone, Yunnan and Vietnam, in the continental extrusion of SE Asia. J. Geol. Soc. 163, 1025–1036.

Song, P., Ding, L., Zhao, T., Li, J., Yue, Y., Xie, J., 2022. Paleomagnetism and geochronology of upper Eocene volcanic rocks from the western Qiangtang block: Constraints on the post-collisional shortening in western Tibet. Global Planet. Change 217, 103953.

Spurlin, M.S., Yin, A., Horton, B.K., Zhou, J., Wang, J., 2005. Structural evolution of the Yushu-Nangqian region and its relationship to syncollisional igneous activity, east-central Tibet. Geol. Soc. Am. Bull. 117, 1293–1317.

Studnicki-Gizbert, C., Burchfiel, B.C., Li, Z., Chen, Z., 2008. Early Tertiary Gonjo basin, eastern Tibet: Sedimentary and structural record of the early history of India-Asia collision. Geosphere 4, 713.

Su, T., Spicer, R.A., Li, S.H., Xu, H., Huang, J., Sherlock, S., Huang, Y.J., Li, S.F., Wang, L., Jia, L.B., Deng, W.Y.D., Liu, J., Deng, C.L., Zhang, S.T., Valdes, P.J., Zhou, Z.K., 2018. Uplift, climate and biotic changes at the Eocene-Oligocene transition in south-eastern Tibet. National Sci. Rev. 6, 495–504.

Tanaka, K., Mu, C., Sato, K., Takemoto, K., Miura, D., Liu, Y., Zaman, H., Yang, Z., Yokoyama, M., Iwamoto, H., Uno, K., Otofuji, Y.-I., 2008. Tectonic deformation around the eastern Himalayan syntaxis: constraints from the Cretaceous palaeomagnetic data of the Shan-Thai Block. Geophys. J. Int. 175, 713–728.

Tang, M.Y., Liu-Zeng, J., Hoke, G.D., Xu, Q., Wang, W.T., Li, Z.F., Zhang, J.Y., Wang, W., 2017. Paleoelevation reconstruction of the Paleocene-Eocene Gonjo basin, SE-central Tibet. Tectonophysics 712–713, 170–181.

Tapponnier, P., Peltzer, G., Ledain, A.Y., Armijo, R., Cobbold, P., 1982. Propagating Extrusion Tectonics in Asia - New Insights from Simple Experiments with Plasticine. Geology 10, 611–616.

Tapponnier, P., Zhiqin, X., Roger, F., Meyer, B., Arnaud, N., Wittlinger, G., Jingsui, Y., 2001. Oblique stepwise rise and growth of the Tibet plateau. Science 294, 1671–1677.

Tauxe, L., Watson, G.S., 1994. The Fold Test - an Eigen Analysis Approach. Earth Planet. Sci. Lett. 122, 331–341.

Todrani, A., Speranza, F., D'Agostino, N., Zhang, B., 2021. Post-50 Ma Evolution of India-Asia Collision Zone From Paleomagnetic and GPS Data: Greater India Indentation to Eastward Tibet Flow. Geophys. Res. Lett. 49 (1), 1–16.

Tong, Y.B., Yang, Z., Zheng, L.D., Xu, Y.L., Wang, H., Gao, L., Hu, X.Z., 2013. Internal crustal deformation in the northern part of Shan-Thai Block: New evidence from paleomagnetic results of Cretaceous and Paleogene redbeds. Tectonophysics 608, 1138–1158.

Tong, Y.B., Yang, Z.Y., Gao, L., Wang, H., Zhang, X.D., An, C.Z., Xu, Y.C., Han, Z.R., 2015. Paleomagnetism of Upper Cretaceous red-beds from the eastern Qiangtang Block: Clockwise rotations and latitudinal translation during the India-Asia collision. J. Asian Earth Sci. 114, 732–749.

Tong, Y.B., Yang, Z.Y., Mao, C.P., Pei, J.L., Pu, Z.W., Xu, Y.C., 2017. Paleomagnetism of Eocene red-beds in the eastern part of the Qiangtang Terrane and its implications for uplift and southward crustal extrusion in the southeastern edge of the Tibetan Plateau. Earth Planet. Sci. Lett. 475, 1–14.

Tong, Y.B., Yang, Z.Y., Pei, J.L., Wang, H., Wu, Z.H., Li, J.F., 2021. Crustal Clockwise Rotation of the Southeastern Edge of the Tibetan Plateau Since the Late Oligocene. J. Geophys. Res. Solid Earth 126 (1), 1–16.

Torsvik, T.H., Van der Voo, R., Preeden, U., Mac Niocaill, C., Steinberger, B., Doubrovine, P.V., van Hinsbergen, D.J.J., Domeier, M., Gaina, C., Tohver, E., Meert, J.G., McCausland, P.J.A., Cocks, L.R.M., 2012. Phanerozoic polar wander, palaeogeography and dynamics. Earth Sci. Rev. 114, 325–368.

Turner, M.B., Cronin, S.J., Stewart, R.B., Bebbington, M., Smith, I.E.M., 2008. Using titanomagnetite textures to elucidate volcanic eruption histories. Geology 36 (1), 31–34.

Vaes, B., van Hinsbergen, D.J.J., van de Lagemaat, S., van der Wiel, E., Lom, N., Advokaat, E., Boschman, L., Gallo, L., li, S., Greve, A., Guilmette, C., Lippert, P., Montheil, L., Langereis, C., 2023. A global apparent polar wander path for the last 320 Ma calculated from site-level paleomagnetic data. Earth Sci. Rev. 245, 104547.

Vaes, B., Li, S.H., Langereis, C.G., van Hinsbergen, D.J.J., 2021. Reliability of palaeomagnetic poles from sedimentary rocks. Geophys. J. Int. 225, 1281–1303.
Vaes, B., Gallo, L.C., Hinsbergen, D.J.J., 2022. On pole position: causes of dispersion of the paleomagnetic poles behind apparent polar wander paths. J. Geophys. Res. Solid Earth 127 (4), 1–22.
van Hinsbergen, D.J.J., 2022. Indian Plate paleogeography, subduction, and horizontal underthrusting below Tibet: paradoxes, controvercies, and opportunities. Natl. Sci. Rev. 9 (8), nwac074.
van Hinsbergen, D.J.J., Kapp, P., Dupont-Nivet, G., Lippert, P.C., DeCelles, P.G., Torsvik, T.H., 2011a. Restoration of Cenozoic deformation in Asia and the size of Greater India. Tectonics 30, TC5003.
van Hinsbergen, D.J.J., Steinberger, B., Doubrovine, P.V., Gassmöller, R., 2011b. Acceleration and deceleration of India-Asia convergence since the Cretaceous: Roles of mantle plumes and continental collision. J. Geophys. Res. Solid Earth 116, B06101.
van Hinsbergen, D.J.J., Lippert, P.C., Dupont-Nivet, G., McQuarrie, N., Doubrovine, P. V., Spakman, W., Torsvik, T.H., 2012. Greater India Basin hypothesis and a two-stage Cenozoic collision between India and Asia. Proc. Natl. Acad. Sci. 109, 7659–7664.
van Hinsbergen, D.J.J., Lippert, P.C., Li, S., Huang, W., Advokaat, E.L., Spakman, W., 2019. Reconstructing Greater India: Paleogeographic, kinematic, and geodynamic perspectives. Tectonophysics 760, 69–94.
XGS (Xizang Geological Survey), 2007, Geological map (1:250000) of the People's Republic of China-Mangkang Country sheet, Wuhan: China University of Geosciences Press. (In Chinese).
Xiong, Z.Y., Ding, L., Spicer, R.A., Farnsworth, A., Wang, X., Valdes, P.J., Su, T., Zhang, Q.H., Zhang, L.Y., Cai, F.L., Wang, H.Q., Li, Z.Y., Song, P.P., Guo, X.D., Yue, Y.H., 2020. The early Eocene rise of the Gonjo Basin, SE Tibet: From low desert to high forest. Earth Planet. Sci. Lett. 543, 116312.
Yan, M.D., Zhang, D.W., Fang, X.M., Ren, H.D., Zhang, W.L., Zan, J.B., Song, C.H., Zhang, T., 2016. Paleomagnetic data bearing on the Mesozoic deformation of the Qiangtang Block: Implications for the evolution of the Paleo- and Meso-Tethys. Gondw. Res. 39, 292–316.
Yang, Z.Y., Yin, J.Y., Sun, Z.M., Otofuji, Y., Sato, K., 2001. Discrepant Cretaceous paleomagnetic poles between Eastern China and Indochina: a consequence of the extrusion of Indochina. Tectonophysics 334, 101–113.
Yin, A., Harrison, T.M., 2000. Geologic evolution of the Himalayan-Tibetan orogen. Annu. Rev. Earth Planet. Sci. 28, 211–280.
Yu, L., Yan, M., Domeier, M., Guan, C., Shen, M., Fu, Q., Xu, W., Xu, Z., Niu, Z., Yang, L., Shi, R., Zhang, W., Zan, J., Zhang, D., Li, B., 2022. New Paleomagnetic and Chronological Constraints on the Late Triassic Position of the Eastern Qiangtang Terrane: Implications for the Closure of the Paleo-Jinshajiang Ocean. Geophys. Res. Lett. 49 (2), 1–12.
Zhang, Y., Huang, W.T., Huang, B.C., van Hinsbergen, D.J.J.v., Yang, T., Dupont-Nivet, G., Guo, Z.J., 2018. 53-43 Ma Deformation of Eastern Tibet Revealed by Three Stages of Tectonic Rotation in the Gongjue Basin. J. Geophys. Res. Solid Earth 123, 3320-3338.
Zhang, W.L., Fang, X.M., Zhang, T., Song, C.H., Yan, M.D., 2020. Eocene Rotation of the Northeastern Central Tibetan Plateau Indicating Stepwise Compressions and Eastward Extrusions. Geophys. Res. Lett. 47.
Zhang, B., Zhang, J.J., Liu, J., Wang, Y., Yin, C.Y., Guo, L., Zhong, D.L., Lai, Q.Z., Yue, Y.H., 2014. The Xuelongshan high strain zone: Cenozoic structural evolution and implications for fault linkages and deformation along the Ailao Shan-Red River shear zone. J. Struct. Geol. 69, 209–233.
Zijderveld, J.D.A., 1967. A.C. demagnetization of rocks: analysis of results. Dev. Solid Earth Geophys. 3, 254–286.